ELSEVIER

Journal of Alloys and Compounds 330–332 (2002) 547–550

Journal of ALLOYS AND COMPOUNDS

www.elsevier.com/locate/jallcom

Hydrogen absorption and desorption in the binary Ti–Al system

K. Hashi[a,*], K. Ishikawa[a], K. Suzuki[b], K. Aoki[a]

[a]*Kitami Institute of Technology, Kitami Koen-Cho 090-8507, Hokkaido, Japan*
[b]*School of Physics, The University of New South Wales, Sydney 2052, Australia*

Abstract

Binary $Ti_{1-x}Al_x$ alloys were hydrogenated at 5 MPa H_2 pressure at room temperature for 173 ks. Structures and thermal stability of the hydrogenated alloys were investigated by XRD and DSC. The hydrogen absorption and hydrogen desorption behavior were investigated by means of a hydrogen analyzer, DSC and XRD. An fcc type (CaF_2 type) hydride formed for $x=0$, 0.20 and 0.25 and an amorphous hydride for $x=0.30$ and 0.35. That is, off-stoichiometric (Al-rich) Ti_3Al (α_2) amorphized by hydrogen absorption. The amount of hydrogen absorption under the quoted conditions decreased with increasing Al concentration, but the 50% hydrogen desorption temperature T_d increased. The hcp solid solution alloy $Ti_{0.80}Al_{0.20}$ showed the best hydrogen absorption and desorption properties of the $Ti_{1-x}Al_x$ alloys investigated.

Keywords: Hydrogen absorption; Ti_3Al; Amorphous; TDS (thermal desorption spectrum); Intermetallic compounds

1. Introduction

In recent years, new hydrogen absorption alloys with a lightweight and a large hydrogen capacity have been desired earnestly. As well known, hydrogen absorption alloys are often produced by a combination of a hydride forming and a non-hydride-forming element. The Ti–Al system is a potential hydrogen absorber because one of its components is lightweight and it contains hydride-forming Ti and non-hydride-forming Al. For instance, when $D0_{19}$-Ti_3Al absorbs hydrogen of 1.45 (H/M) (3.32 mass%) it changes to an fcc type hydride (CaF_2 type); however, the hydrogen desorption temperature is too high to use for practical applications [1]. Reducing the hydrogen desorption temperature is one of the most important problems to be solved for the Ti–Al–H system. Although hydrogen absorption and desorption properties of stoichiometric Ti_3Al and its hydride structure have been investigated by several research groups [1–8], little work has been done on a compositional dependence. As the Al concentration increases in the Ti–Al system, it is expected that the hydrogen absorption capacity decreases and the hydrogen desorption temperature reduces. In the present work, the structural changes caused by hydrogenation, the hydrogen absorption capacity and hydrogen desorption behavior are investigated for the $Ti_{1-x}Al_x$ alloys in order to get information on reducing the hydrogen desorption temperature.

2. Experimental

Binary $Ti_{1-x}Al_x$ (mol%) alloys were prepared by arc melting of titanium (99.8%) and aluminum (99.999%) in an argon atmosphere. The ingots were pulverized and sieved less than 50 mesh. The powder samples were activated at 673 K for 3.6 ks in a vacuum and reacted slowly with extra high purity hydrogen (99.99999%) at room temperature for 173 ks. The structure of the samples before and after hydrogenation was identified by powder X-ray diffraction (XRD) using Cu Kα radiation monochromated by graphite. Thermal stability and structural changes of the hydrogenated alloys were examined with differential scanning calorimetry (DSC) at a heating rate of 0.67 K/s in a flowing argon atmosphere and XRD. The amount of hydrogen absorbed in the samples and thermal desorption spectra (TDS) were monitored by a hydrogen analyzer at a heating rate of 2 K/s.

3. Results and discussion

Fig. 1 shows typical XRD patterns of $Ti_{1-x}Al_x$ alloys (a) before and (b) after hydrogenation. The hydrogen content

*Corresponding author.

0925-8388/02/$ – see front matter
PII: S0925-8388(01)01660-7

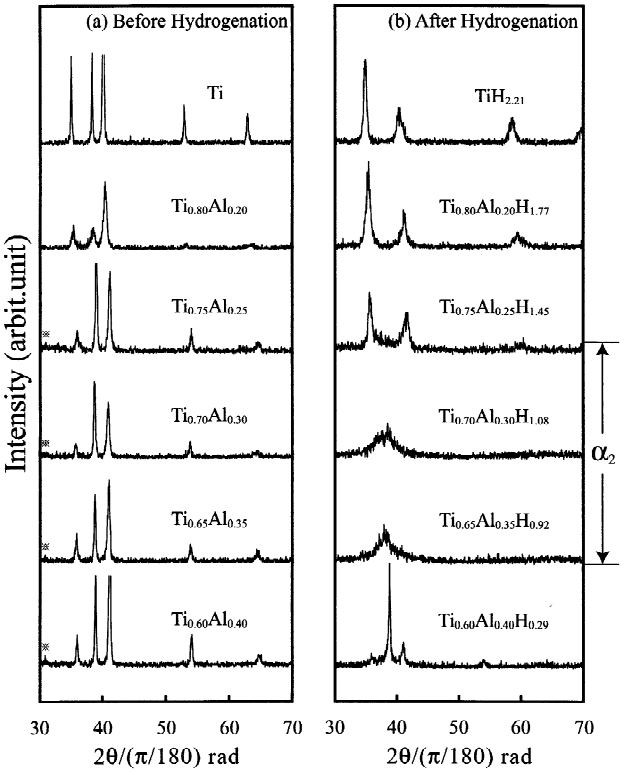

Fig. 1. XRD patterns of $Ti_{1-x}Al_x$ alloys (a) before and (b) after hydrogenation. *Denotes the (110) order Bragg peak.

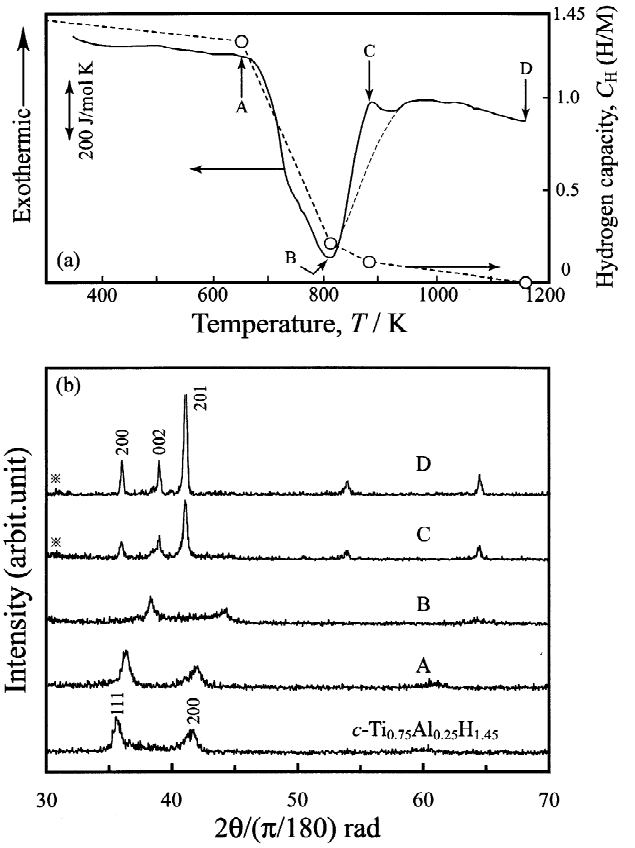

Fig. 2. A DSC curve and a change in the hydrogen content (H/M) (a) in c-$Ti_{0.75}Al_{0.25}H_{1.45}$ and XRD patterns of these samples heated to the distinct stages in DSC (b). *Expresses the (110) order Bragg peak.

is written in the formula given for each alloy. The XRD patterns of both Ti and $Ti_{0.80}Al_{0.20}$ are indexed on the basis of the hcp structure. On the other hand, a weak order (110) Bragg peak (labeled as *) is seen around 32° in the XRD patterns of the alloys for $x=0.25$, 0.30, 0.35 and 0.40. Thus, these alloys have the $D0_{19}$ structure in agreement with the phase diagram [9]. The XRD patterns of hydrogenated $Ti_{1-x}Al_x$ alloys for $x=0$, 0.20 and 0.25 are indexed on the basis of the fcc (CaF_2) type hydride. However, the Bragg peaks disappear and are replaced with a broad maximum in the XRD patterns of hydrogenated alloys for $x=0.30$ and 0.35. The bright field image of TEM for these samples is featureless and the diffraction pattern shows a halo characteristic of an amorphous phase [10]. Furthermore, the DSC curve of these samples shows an exothermic peak of crystallization as will be shown later. Therefore, these alloys are concluded to be amorphous and are expressed as a-$Ti_{0.70}Al_{0.30}H_{1.08}$ and a-$Ti_{0.65}Al_{0.35}H_{0.92}$. The reason why an amorphous phase forms by hydrogenation of Al-rich Ti_3Al is uncertain at the present stage. The XRD pattern of hydrogenated $Ti_{0.60}Al_{0.40}$ shows an amorphous halo overlapping with the Bragg peaks of the hydrogen unabsorbed $D0_{19}$ phase.

Fig. 2 shows a DSC curve and a change in the hydrogen content (H/M) (a) in crystalline c-$Ti_{0.75}Al_{0.25}H_{1.45}$ and XRD patterns (b) of these samples heated to the distinct stages shown in the DSC curve. The hydrogen content in c-$Ti_{0.75}Al_{0.25}H_{1.45}$ decreases with increasing temperature, especially rapidly between the A and the B point. Therefore, a prominent endothermic peak around 800 K is due to hydrogen desorption. The fcc-$Ti_{0.75}Al_{0.25}H_{0.21}$ (heated to the B point) transforms to $D0_{19}$-$Ti_{0.75}Al_{0.25}H_{0.11}$ on heating to the C point. Therefore, a small exothermic peak around the C point overlapped with the endothermic peak is due to the transformation from the fcc to the $D0_{19}$ phase.

Fig. 3 shows a DSC curve and a change in the hydrogen content (H/M) (a) in amorphous a-$Ti_{0.70}Al_{0.30}H_{1.08}$ and XRD patterns (b) of these samples heated to the distinct stages shown in the DSC curve. In comparison with the DSC curve of c-$Ti_{0.75}Al_{0.25}H_{1.45}$, that of a-$Ti_{0.70}Al_{0.30}H_{1.08}$ shows an exothermic peak around 650 K. Since a-$Ti_{0.70}Al_{0.30}H_{1.08}$ transforms to fcc-$Ti_{0.70}Al_{0.30}H_{0.89}$ exothermally on heating from the A to the B point, an exothermic peak around 650 K is concluded to result from crystallization. The fcc-$Ti_{0.70}Al_{0.30}H_{0.27}$ (heated to the C point) transforms to the $D0_{19}$-$Ti_{0.70}Al_{0.30}$ on heating to the D point. Therefore, an exothermic peak around 850 K overlapped with the endothermic peak is due to the transformation from the fcc type hydride to the $D0_{19}$ phase. The present work indicates that a-$Ti_xAl_{1-x}H_y$ crystallizes to the original $D0_{19}$ phase. However, such crystallization is not always common in hydrogen-induced amorphous alloys. For instance, a-RM_2H_x prepared by

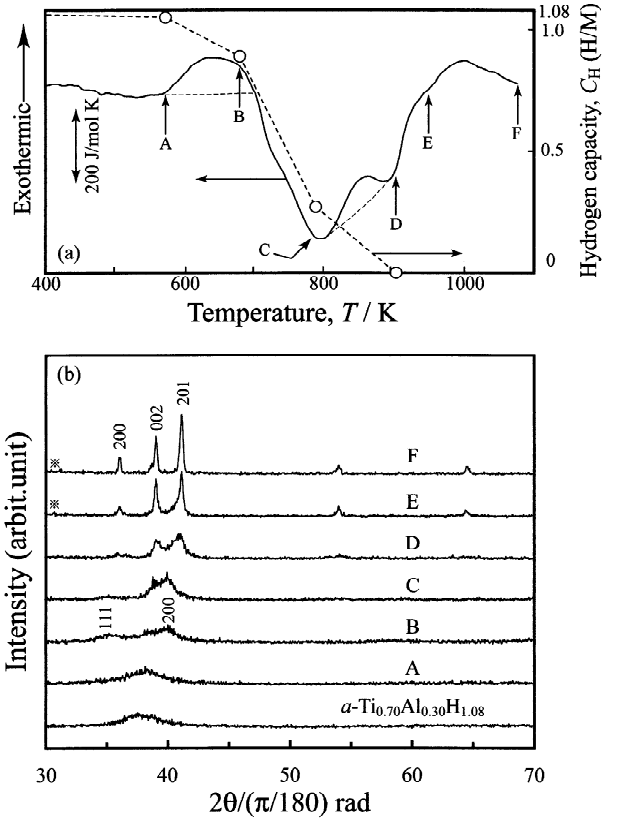

Fig. 3. A DSC curve and a change in the hydrogen content (H/M) (a) in a-$Ti_{0.70}Al_{0.30}H_{1.08}$ and XRD patterns of these samples heated to the distinct stages in DSC (b). *Expresses the (110) order Bragg peak.

hydrogenation of C15 Laves RM_2 (M=Fe, Co, Ni; R=a rare earth metal) crystallize into RH_2 and M [11]. That is, disproportionation occurs at elevated temperatures. Consequently, reversible hydrogen absorption and desorption is impossible in a-RM_2H_x. On the contrary, since a-Ti_3AlH_x crystallizes to the original $D0_{19}$ structure, i.e., returns to the original phase, reversible hydrogen absorption and desorption are possible.

Fig. 4 shows thermal desorption spectra (TDS) of the hydrogenated $Ti_{1-x}Al_x$ alloys. Hydrogen desorption from two or three distinct trap states is seen. These trap states are labeled from low temperature to high temperature as #1, #2, and #3. General known features of the desorption rate of hydrogen versus temperature are: (1) as the binding energy of a trap state is increased, the desorption peaks occurs at more elevated temperatures, (2) an increased trap state density (i.e., an increased hydrogen concentration) is given by an increased area under the desorption peak, and (3) as the heating rate is increased, the desorption peaks are displaced to higher temperatures and the corresponding peak flux is higher. Therefore, the lowest temperature peak around 550–600 K may result from hydrogen desorption trapped in more unstable sites. It is worth noticing that the low temperature peak around 500–600 K in c-$Ti_{1-x}Al_xH_y$ disappears in the TDS of a-$Ti_{1-x}Al_xH_y$, suggesting that

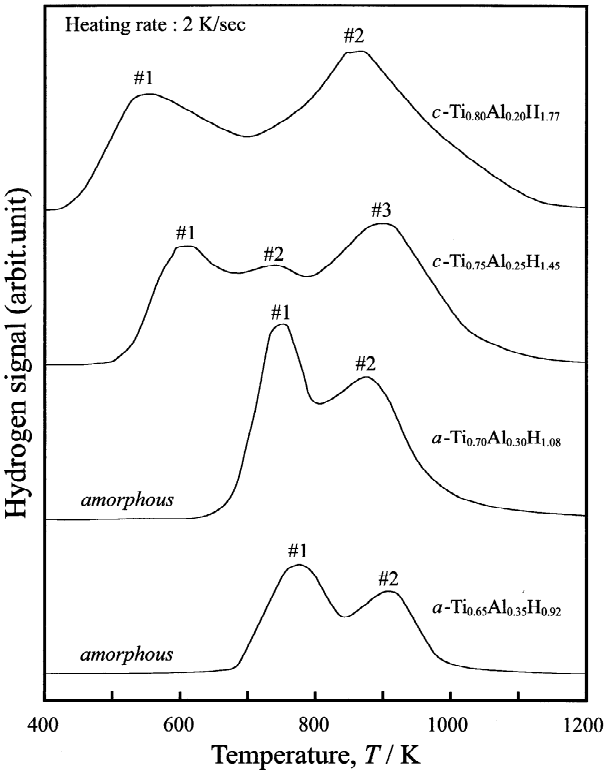

Fig. 4. Thermal desorption spectra (TDS) of c- and a-$Ti_{1-x}Al_xH_y$ heated by 2 K/s.

hydrogen in a-$Ti_{1-x}Al_xH_y$ occupy more stable occupation sites than those in c-$Ti_{1-x}Al_xH_y$.

Fig. 5 shows the amount of hydrogen absorption for

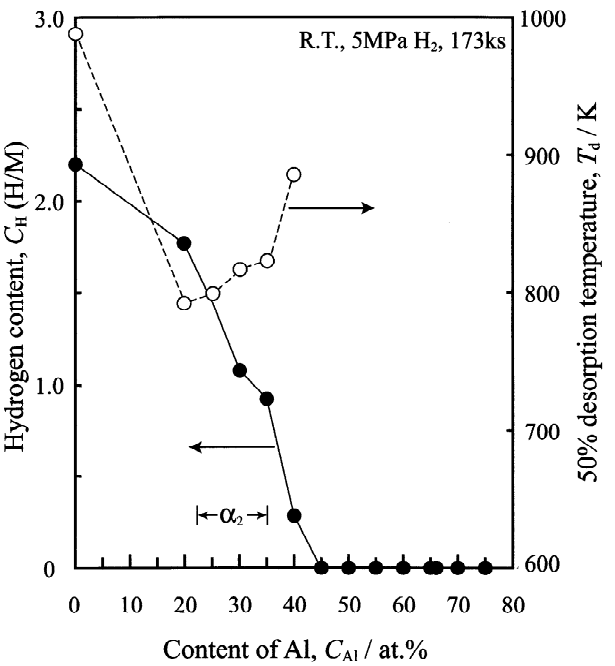

Fig. 5. The amount of hydrogen absorbed at 5 MPa for 173 ks at room temperature and the 50% hydrogen desorption temperature T_d plotted against the Al concentration.

room temperature and 5 MPa for 173 ks, expressed as the atomic ratio of hydrogen to metal (H/M), together with the 50% hydrogen desorption temperature, T_d, plotted against the Al concentration. Because the number and the shape of the TDS peaks vary with the Al concentration, it is difficult to evaluate the hydrogen desorption ability. Instead, the temperature at which a half amount of absorbed hydrogen is desorbed is defined for convenience as the 50% hydrogen desorption temperature T_d in the present work. Pure Ti and hcp-solid solution alloy $Ti_{0.80}Al_{0.20}$ absorb hydrogen of 2.21 (H/M) (4.44 mass %) and 1.77(H/M) (3.93 mass %), respectively. T_d values of Ti and $Ti_{0.80}Al_{0.20}$ are 983 K and 787 K, respectively. As the Al concentration increases, the amount of hydrogen absorption decreases, but T_d decreases at first and increases above $x=0.2$ contrary to our expectation. That is, T_d shows a minimum at approximately $Ti_{0.80}Al_{0.20}$. Here, we must take note of the fact that hydrogenated off-stoichiometric (Al rich-) Ti_3Al are amorphous. No hydrogen is absorbed in the alloys for $x>0.45$. That is, the other intermetallic compounds $L1_0$-TiAl, Al_2Ti and Al_3Ti do not absorb hydrogen. From Fig. 5, we can see that hcp solid solution alloy $Ti_{0.80}Al_{0.20}$ has the best hydrogen absorption and desorption properties under the present experimental conditions.

4. Summary and conclusions

Under the conditions for hydrogen absorption in our experiments, stoichiometric Ti_3Al changes from the $D0_{19}$ structure to the fcc type hydride Ti_3AlH_x. However, off-stoichiometric (Al-rich) Ti_3Al, i.e., $Ti_{0.70}Al_{0.30}$ and $Ti_{0.65}Al_{0.35}$ change to amorphous a-Ti_3AlH_x alloys. Pure Ti absorbs hydrogen of 2.21 (H/M) and changes to the fcc type hydride (CaF_2) TiH_2. The amount of hydrogen content decreases with increasing the Al content, but T_d decreases at first and then increases above $x=0.20$. The hcp solid solution alloy $Ti_{0.80}Al_{0.20}$ has the best hydrogen absorption and desorption properties under the present experimental conditions.

Acknowledgements

This work was supported in part by a Grant-in-Aid for Scientific Research on Priority Areas A of ‘New Protium Function’ from the Ministry of Education, Science, Sports and Culture.

References

[1] P.S. Rudman, J.J. Reilly, R.H. Wiswall, J. Less-Common Met. 58 (1978) 231.
[2] D.S. Schwartz, W.B. Yelon, R.R. Berliner, R.J. Lederich, S.M.L. Sastry, Acta Metall. Mater. 39 (1991) 1977.
[3] A. Takasaki, Y. Furuya, J. Alloys Comp. 292 (1999) 287.
[4] W.-Y. Chu, A.W. Thompson, J.C. Williams, Acta Metall. Mater. 40 (1992) 455.
[5] A. Takasaki, Y. Furuya, Y. Taneda, Mater. Sci. Eng. A239–240 (1997) 265.
[6] D. Sonadurai, B.K. Panigrahi, V.S. Sastry, Ramani, J. Alloys Comp. 289 (1999) L1.
[7] D. Eliezer, T. Haddad, M. Dagur, F.H. Froes, Scripta Metall. Mater. 27 (1992) 845.
[8] D.S. Shih, G.K. Scarr, G.E. Wasieleski, Scripta Metall. 23 (1989) 973.
[9] T.B. Massalski, H. Okamoto, P.R. Subramanian, L. Kacprzak, in: Binary Alloy Phase Diagrams, 2nd Edition, American Society for Metals, Metals Park, OH, 1990.
[10] K. Hashi, K. Ishikawa, K. Suzuki, K. Aoki, Scripta Materia. 44 (11) (2001) 2591.
[11] K. Aoki, T. Yamamoto, Y. Satoh, K. Fukamichi, T. Masumoto, Acta Metall. 35 (1987) 2465.